

## **Bending Deformation of Bio-tensegrity Model at Different Deployable Schemes**

Nur Syakinah Anuar<sup>1</sup>, Balqis Md Yunus<sup>1\*</sup>, Nadiah Saari @ Ash'ari<sup>1</sup>, Syed Muhammad Syed Yahya<sup>2</sup>, Oh Chai Lian<sup>1</sup>

<sup>1</sup>School of Civil Engineering, College of Engineering, Universiti Teknologi MARA, 40450, Shah Alam, Selangor, Malaysia

<sup>2</sup>School of Civil Engineering, College of Engineering, Universiti Teknologi MARA, 81750, Masai, Johor, Malaysia

\*Corresponding author: balqis1157@uitm.edu.my

Received: 08 June 2023/ Accepted: 30 October 2023 / Published online: 29 March 2024

---

### **Abstract**

Tensegrity structures consist of multiple struts or cables that are interconnected and ideal for deployable structures. Given the challenges of controlling the strut's deformation, active cables are more preferred and commonly studied in the deployment of tensegrities. The selection of the active cables becomes important as the deployment of tensegrities is highly dependent on the construction cost and computational time. This paper presents three different deployable schemes considering different sets of active cables. The deployable schemes were studied in this study to investigate the bending deformation of a human spine-inspired bio-tensegrity model. The shape change strategy involves a computational approach based on sequential quadratic programming to optimise the cable force elongation. A total of nine shape change analysis cases were conducted on the bio-tensegrity model to undergo deformation under three different schemes and three uni-directional targeted coordinates. The bending ability of bio-tensegrity models, the convergence curve, and axial forces were all discussed. It was found that the deployment scheme S3 is the most efficient scheme for the model to achieve different targets in uni-directional mode. This study is useful for applications such as deployable structures, automation, and robots.

**Keywords:** Bio-tensegrity; Bending deformation; Deployable; Optimisation; Shape change analysis

---

### **1. Introduction**

Civil engineering structures are meticulously engineered to endure projected loads throughout their operational lifespan. However, instances arise where supplementary support becomes necessary for lightweight structures or those that have experienced a decline in load-bearing ability due to factors such as natural calamities or ageing. This augmentation aims to provide temporary bolstering and to furnish an advanced alert mechanism, preventing excessive deformation by tapping into substantial deformation reserves and interconnectivity redundancy. Consequently, a growing interest in deployable systems has been observed in civil engineering structures due to their versatility to change the shape by folding, sliding and rotating with detachable features to ease transportation and storage (Chen et al., 2018; Shang et al., 2018; Shi et al., 2018; Liu et al., 2020; Phocas et al., 2020).

The tensegrity principle is one of the prominent approaches for incorporating it into the design of deployable structures (Kan et al., 2018). Tensegrity has been used in many fields, including neurology, orthopaedics, robotics, etc. Moreover, the architectural industry has also shown a rising interest in the cutting-edge characteristics of deployable structures and the intent to introduce tensegrity entities into real-world structures. Tensegrity's elements can be programmed to be sensors, actuators, or load-bearing elements and can control the electrical, thermal, and energy stored in the system (Oh et al., 2012). This technology can cater to the requirements of loading variation, environment variations (i.e., temperature, solar path movement), settlement and damage occurrence for design structures in civil engineering.

Tensegrity is a design principle defined as a pin-jointed system that consists of cables (elements in tension) and struts (elements in compression). The compressive elements are discontinuous in classic tensegrity structures and they float in a continuous network of tension elements. Tensegrity has infinitesimal mechanisms balanced with a self-stress state (Pellegrino and Calladine, 1986; Motro, 2011; Snelson, 2012). Tensegrity systems have a very good stiffness-to-mass ratio and are prone to structural control through an adjustment of self-stress forces (Al-Sabouni et al., 2018). The parameters of the unfolded structure and its deployment can be controlled using only selected, so-called active members, which are a big advantage as they reduce the number of actuators. They can be folded and unfolded in many ways: by modifying the lengths of struts, cables, or both, using a bundle or plane-type folding. Apart from changing configurations, the pin-jointed connection between the tensegrity elements promotes spatial structure. Owing to their tightly interconnected members, tensegrity structures provide an arena for the exploration of cutting-edge control algorithms designed for deployment (Sultan and Skelton, 2003).

Tensegrity structures represent lightweight and adaptable frameworks that find valuable applications in diverse scenarios, including flat roofs (Csölleová, 2012), floors (Fest et al., 2004; Motro et al., 2006), shells (Skelton et al., 2001), and towers (Schlaich, 2003). The presence of self-stress is vital to the integrity of tensegrity structures, as its absence renders the structure inherently unstable, succumbing to internal mechanisms (Schenk et al., 2007). To manipulate and regulate these structures, two primary strategies have emerged. One involves the activation of struts for shape control (Averseng and Dubé, 2012; Amendola et al., 2014), while the other entails the actuation of cables to achieve the desired structural configurations (Sultan, 2014). This deliberate manipulation of components opens avenues for intricate and precise control of tensegrity structures' overall geometry and behaviour.

Bio-tensegrity is a new concept that provides optimum solutions to the current demands of structures' flexibility and resilience. Bio-tensegrity is the creation of structures that are inspired by biological systems, such as the anatomy and physiology of the human body. The principle of bio-tensegrity has also been widely used in fields of medical technology, automation manufacturing and bio-tensegrity robots in the construction industry. The terminology suggests applying the tensegrity concept by identifying the interaction of forces in a hierarchical biological system (Oh et al., 2019). Past research has initiated bio-tensegrity that can replicate the spine, foot, elbow, and DNA (Swanson, 2013). Flexural joints of bio-tensegrity structures enable them to disperse load across the entire system. Additionally, the anatomical shape of the human joint would adjust its impact on external forces, permitting it to function in unpredictable settings (Jung et al., 2018).

The shape of the bio-tensegrity spine model also accentuates the slenderness and curvature, promoting various shape changes that could be made (Oh et al., 2020). However, multiple degrees of freedom deployment have remained intangible, with small deformations recurrently used in research on the active control of tensegrity structures. Therefore, complex deployment tasks are rarely assessed on near-full-scale structures. In the present paper, the authors propose and analyse the bending deformation of a tensegrity model at various deployable schemes. The proposed tensegrity model used in this study was inspired by biological principles, using the human spine model to evaluate the possible series of moveable mechanisms for a deployable structure. The human spine emphasises the musculoskeletal interaction of the muscles and spinal column arrangement. The model can be visualised as the interaction between cable and struts based on vertebrae and muscles in the human

body. Using numerical analysis, several constraint parameters and assumptions were imposed on the model at various schemes.

## 2. Methods

A bio-tensegrity model was analysed in three different deployment schemes and three uni-directional targeted coordinates. The deployment scheme encompasses both the undeformed diagonal cables and the cables that are allowed to have forced elongation. At the end of the shape change analysis, the monitored nodes will advance and reach the prescribed targeted coordinates.

### 2.1 Geometry

The adaptation of the geometrical bio-tensegrity model in this study was the continuation of research on spine bio-tensegrity models by Oh et al. (2020). The bio-tensegrity model inspires the human spine due to its natural curvature, allowing for shape deformation by incorporating vertebrae's movements at certain postures. The tips and vertices of each spine's region curvatures were used to idealise the topology of the spine-bio-tensegrity model.

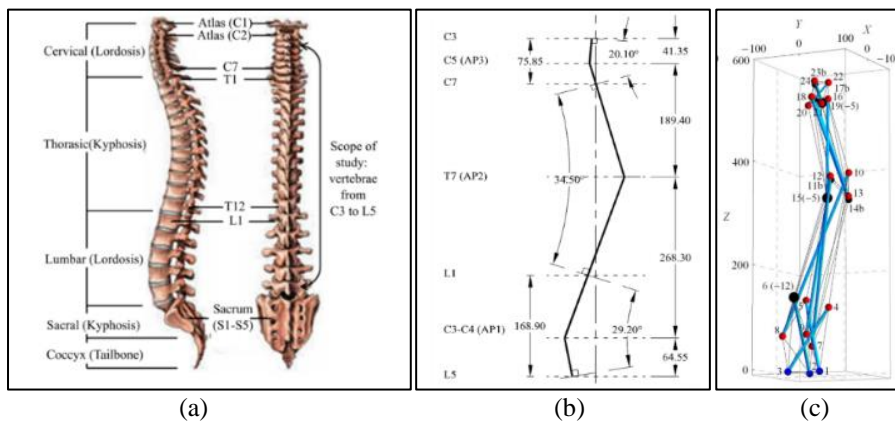


**Figure 1.** (a) Spine anatomy, (b) Spine curvature idealisation, (c) Self-equilibrated spine bio-tensegrity model (Oh et al. 2020)

Figure 1 shows the establishment of the self-equilibrated spine bio-tensegrity model mimicking the human spine. The model consists of 24 nodal coordinates in a three-dimensional Cartesian plane and comprises 69 elements of the struts and cables. Table 1 shows the nodal coordinates of the spine bio-tensegrity model measured in units of *mm*.

**Table 1.** Nodal coordinates of spine bio-tensegrity model (Unit in *mm*)

Node	<i>x</i>	<i>y</i>	<i>z</i>	Node	<i>x</i>	<i>y</i>	<i>z</i>
1	9.33	-1.23	0	13	14.15	63.71	332.85
2	-35.34	-45.27	0	14	-24.57	45.65	332.85
3	26	-61.7	0	15	10.42	16.15	332.85
4	-8.9	9.49	123.78	16	-5.08	10.05	531.04
5	-25.95	-48.49	141.36	17	-13.91	-22.77	533.31
6	34.85	-44.2	141.36	18	18.99	-13.96	533.31
7	-33.22	-39	52.83	19	-18.29	-9.79	527.57
8	8.47	-82.75	70.41	20	4.74	-28.59	519.59
9	24.76	-21.96	70.41	21	13.56	4.31	519.59
10	-10.04	52.87	382.82	22	-7.58	9.77	564.29
11	-14.34	11.56	372.81	23	-10.33	-21.21	564.29
12	24.38	29.61	372.81	24	17.91	-8.04	564.29

## 2.2 Shape Change Method

The self-equilibrate human spine bio-tensegrity model undergoes 4 stages in the shape change strategy: the initial stage, the deformed stage, the shape change stage and the final stage. The bio-tensegrity model, without loads, acquires self-stress at the initial stage and starts to deform when it is under loading and constraints at the deformed stage. During the shape-change stage, the bio-tensegrity model searches for an appropriate path to reach the targeted coordinates by going through a number of iterations. The actuation of the model focused only on the uni-directional displacement of 3 top monitor nodes (*x*, *y*, and *z*): Node 22 (-7.58, 9.77, 564.29), Node 23 (-10.33, -21.21, 564.29) and Node 24 (17.91, -8.04, 564.29). The numerical analysis of this study follows several assumptions due to the model's limitations and the mathematical programming (Oh et al. 2019).

### 2.2.1 Shape Change Algorithm

Shape change analysis for this model was performed based on the algorithm from Oh et al. (2019) as shown in Figure 2. The shape-change algorithm was built based on two important algorithms. Algorithm 1 is the basic algorithm demonstrating the overall shape change computationally for the tensegrity model. Meanwhile, Algorithm 2 is the loop process for finding the optimum forced elongation. In order to mimic the shortening or extension of human muscles to deploy a human spine, only cables are allowed for forced elongation in the shape change analysis. In Algorithm 2, the sequential quadratic programming (SQP) method is used to solve the nonlinear optimisation problem. The forced elongation of a cable is calculated by solving the quadratic programming sub-problem with inequality constraints as expressed in Equation 1:

$$\begin{aligned} \min_{x \in R^n} f(x) &= \mathbf{g}^T \mathbf{t} \mathbf{l} + \frac{1}{2} \mathbf{t}^T \mathbf{H} \mathbf{t} \mathbf{l} \\ \text{subject to } & \mathbf{A}_2 \mathbf{t} \mathbf{l} \geq \mathbf{b}_2 \end{aligned} \quad (1)$$

where  $\mathbf{g}$  is vector of distance between monitored node and target coordinates,  $\mathbf{t}$  is vector of incremental forced elongation, which corresponds to the optimisation variable and  $\mathbf{H}$  is a positive-definite approximation of Hessian matrix of the Lagrangian function. Matrix  $\mathbf{A}_2$  and vector  $\mathbf{b}_2$  are the inequality constraints corresponding to the limitations in allowable axial forces and forced elongation, respectively. The updated nodal coordinates

and axial forces at every incremental step  $t=i$  are determined based on the optimised forced elongation of cables. The objective function in Algorithm 1 is calculated as follows:

$$\min f(x) = |{}^t x - {}^f x| \tag{2}$$

where  ${}^f x$  is the prescribed target coordinates, and  ${}^t x$  is the current coordinates, for all the specified monitored nodes at the current step  $t$  during the shape change analysis. The satisfaction of termination criteria is checked for compliance with the termination criteria of (i) objective function in Eqn. 2 or (ii) maximum iteration being greater than 10000. If the analysis meets either one of these criteria, Algorithm 1 will be terminated, indicating the end of the shape change analysis.

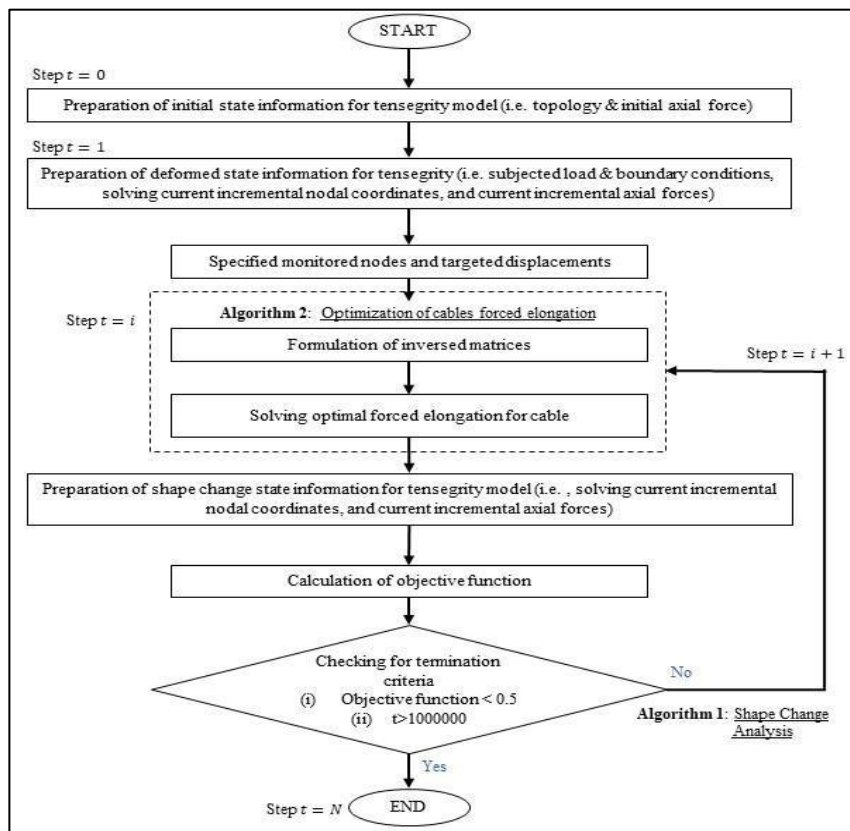


**Figure 2.** Shape change algorithm (Oh et al., 2019)

The shape-change analysis was performed using Fortran programming. An input file was first prepared based on the nodal coordinates, element connectivity, material properties, loading, constraints, monitor nodes and targeted coordinates of a bio-tensegrity model. In Fortran programming, the main program detailed the overall computational process for the shape change analysis. The Flop program was built to read the input file for the shape change analysis. The shape change analysis for the spine bio-tensegrity model was built, run, and executed using Fortran's programming. The data collections on shape change illustrations, axial loads and

convergence were later retrieved from the output program, which was automatically generated after the program was executed.

### 2.2.2 Deployable Scheme

In this study, only cables encounter forced deformation (i.e., active cables), while the struts at elastic deformation. The sets of passive cables (i.e., those not undergoing forced elongation) that distinguish the three deployment schemes of the bio-tensegrity model under investigation in this study. Table 2 shows the deployable schemes and the selected passive cables. The deployable schemes 1, 2 and 3 are associated with the passive cables selected from diagonal cables at stage 1, stage 2 and stage 3, respectively. Three top nodes, namely Node 22, Node 23, and Node 24, are defined as monitor nodes. These nodes were monitored to achieve the prescribed targeted coordinates. Table 3 presents nine (9) analysis cases with the targeted coordinates set at  $x$ -direction in uni-directional mode of 200 mm, 400 mm and 600 mm away from the initial positions. The shape change analysis stops at the final stage when the monitor nodes achieve the targeted coordinates. Figure 3 shows the positions of the passive cables in three deployment schemes.

**Table 2.** Different deployment schemes and its cable groups

Deployable Scheme	Passive cables group
Scheme 1, S1	Diagonal cables 1, S1
Scheme 2, S2	Diagonal cables 2, S2
Scheme 3, S3	Diagonal cables 3, S3

**Table 3.** Target coordinates

Uni-directional incremental (in mm)	Monitored coordinates		
	Node 22 $X_{22}=-7.58$	Node 23 $X_{23}=-10.33$	Node 24 $X_{24}=17.91$
	Target coordinates		
$x = 200$	192.42	189.67	217.91
$x = 400$	392.42	389.67	417.91
$x = 600$	592.42	589.67	617.91

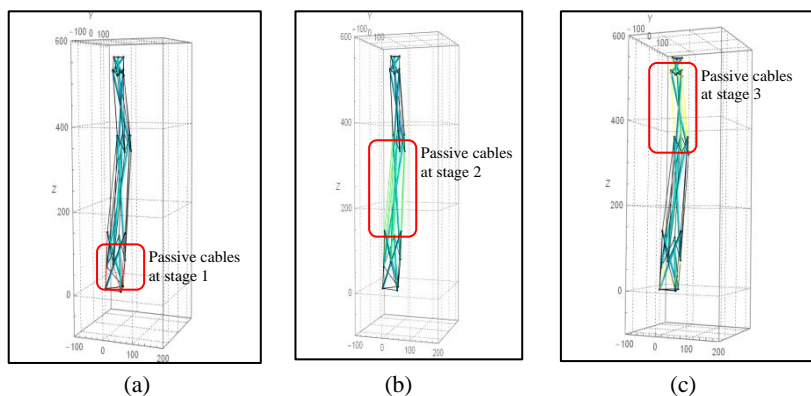


**Figure 3.** Deployable schemes; (a) Scheme 1 (b) Scheme 2 (c) Scheme 3

### 3. Results and Discussion

#### 3.1 Shape Change Configuration at Different Target Displacements

All monitored nodes have successfully reached their targeted nodes in all schemes. Only randomly chosen cases are presented in this paper to show the shape change of the spine bio-tensegrity model at different target displacements, as shown in Figure 4. The incremental shape change is demonstrated at the initial step, 50% of the computational and final steps. The observation has been made, and it is found that the model experienced cable twisting, rotation, extension, and contraction throughout the shape change procedures. They experienced a decline in height from the initial as they approached the prescribed targeted nodes. The analysis cases with target displacements of 600 mm (i.e., S1X600, S2X600 and S3X600) undergo a shortened more than 60% from the initial height at the final steps. Meanwhile, the cases with target displacements of 400 mm (i.e., S1X400, S2X400 and S3X400) experienced about 40-50% height reduction. The cases with a target displacement of 200 mm (i.e. S1X200, S2X200 and S3X200) only decreased around 10-20% from the original height. Apart from having the changes in height, the model in all analysis cases demonstrates the bending deformations. It is noted that the potential of the spine bio-tensegrity model to perform bending deformation is mainly attributed from the target displacements prescribed in the  $x$ -direction (see Table 3).

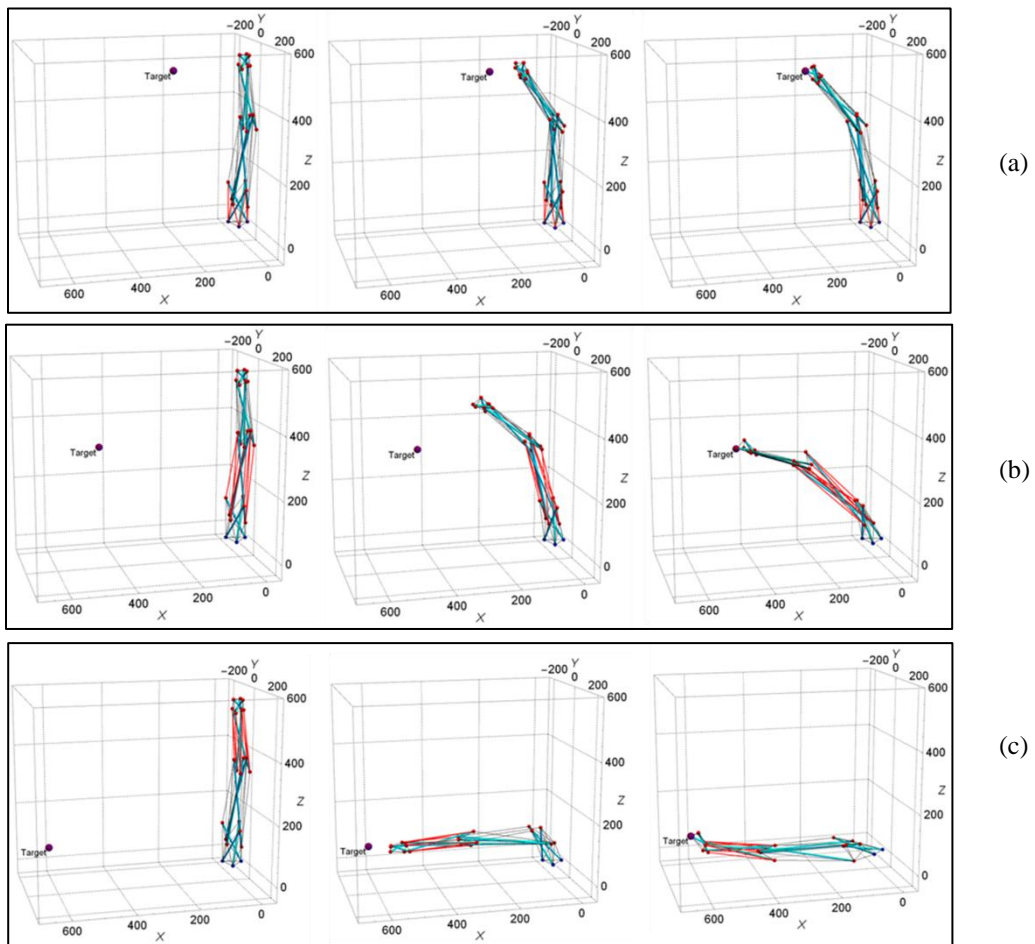


**Figure 4.** Different targeted displacements for (a) case S1X200, (b) case S2X400 and (c) case S3X600.

### 3.2 Shape Change at Different Deployment Schemes

This section explains in detail the shape change of the model at different deployment schemes. The shape changes of the initial and final stages of the analysis cases S1X200, S2X200 and S3X200 were presented and discussed. Case S1X200 was observed to contract the diagonal cables at stage 2 to actuate the model system to sideways. The deployment path for Scheme 1 continued to rotate clockwise. A few steps before reaching the final coordinates, the model twisted to advance to the final coordinates.

Case S2X200 was displaced during the deployment process by extending the group of diagonal cables at stage 1 outward. This induced a reduction in the height of the overall model. The group of diagonal cables at stages 3 and 4 had elongated excessively in order for the monitored nodes to reach the pre-determined coordinates. The rotation of the model at Scheme 2 deployment is not significant.

Case S3X200 initiated the displacement towards the targeted nodes by folding several cables in diagonal cable stage 1. Approaching the halfway shape change process, the model was observed to start twisting with the gradual extension of the group of diagonal cable stage 4 and top horizontal cables. On the overall observation of case S3X200, there is an obvious clockwise rotation when approaching the target (i.e., after step  $t = 10$ , and the final step is 13).

Overall, shape change analysis of the bio-tensegrity model at different schemes still indicates the models undergo bending deformation in the x-direction. The model generally experienced a reduction in heights to displace at prescribed coordinates. On the other hand, the best fit for deployment of the spine bio-tensegrity model's scheme should be the model with fewer computational steps, which is Scheme S3.

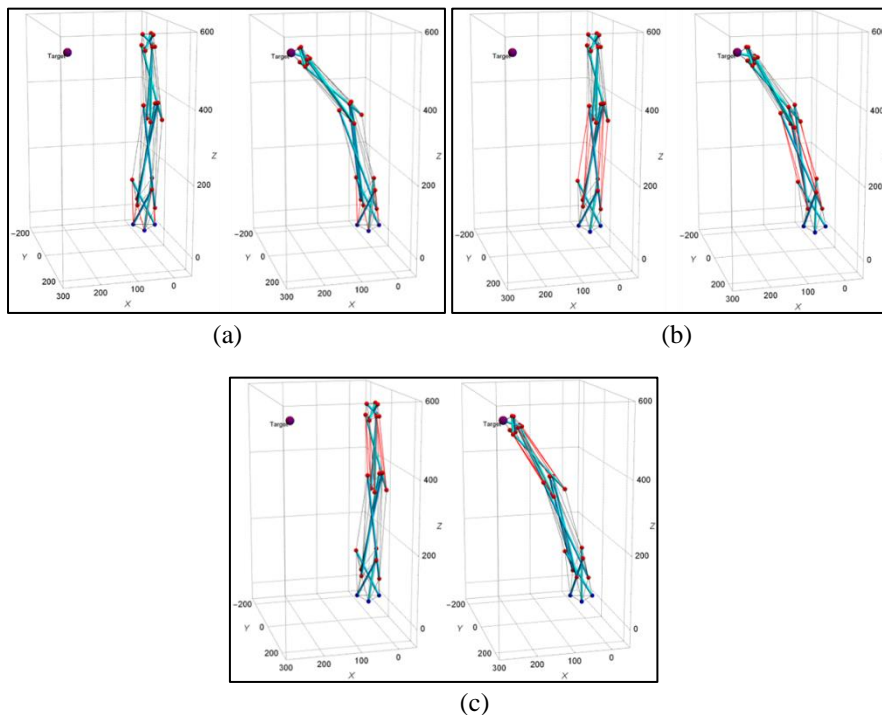


**Figure 5.** Different deployment schemes for (a) case S1X200, (b) case S2X200 and (c) case S3X200.

### 3.4 Convergence

The convergence curve represents the computational efficiency of the model in the control parameter to achieve the pre-determined target. All the models' monitored nodes were subjected to one degree of freedom (DOF) in uni-directional displacement in the x-direction. The spine bio-tensegrity models Scheme 1, Scheme 2 and Scheme 3 are allowed to deform in a positive x-direction, denoted by S1, S2 and S3 respectively.

The magnitude of the final coordinates is specified with +200 mm increments from the original x-coordinate of monitored nodes. Monitored nodes are located at the top of the model configurations, which involve Node 22, Node 23, and Note 24. Table 4 shows the number of computational steps for shape change analysis using quadratic programming. The models were analysed under the undeformed cable groups of a few schemes. They experienced axial elongation, axial shortening and sideways deformations to achieve the targeted coordinates.

**Table 4.** Numbers of computational steps

Undeformed scheme	Positive increment in the x-direction		
	200mm	400mm	600mm
Scheme 1, S1	16	39	91
Scheme 2, S2	14	31	76
Scheme 3, S3	13	26	73

Figure 4 shows the normalised objective function (NOF) against computational steps for all analysis cases. The convergence trend can be compared between analysis cases when the NOF for each case is constructed with the maximum objective function in Equation 2 set at 1.0. All the convergence curves show a declining trend approaching the final coordinates. For the models subjected to small displacement (at  $x = +200$  mm, i.e., S1X200, S2X200 and S3X200), the curves were relatively decreased almost linearly compared to other displacement values.

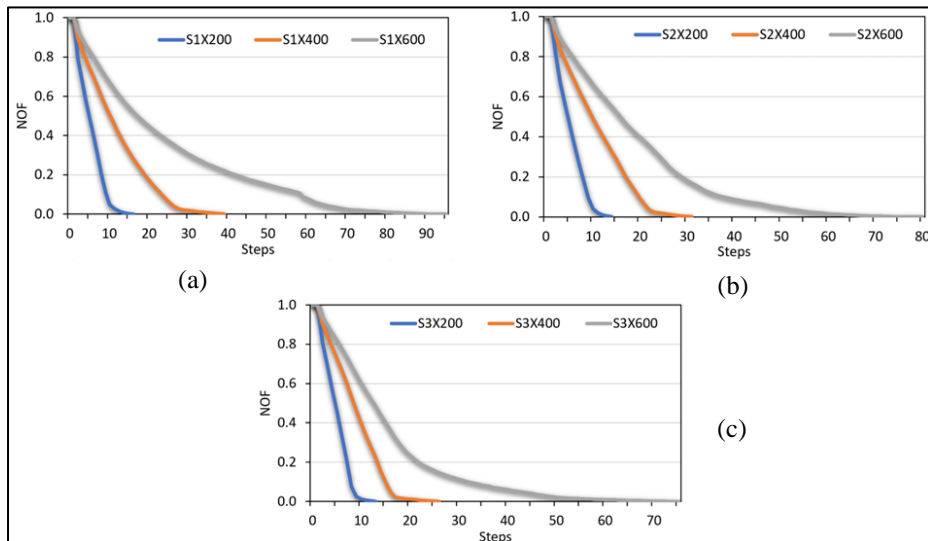


**Figure 4.** Convergence curves for (a) Scheme 1, (b) Scheme 2, and (c) Scheme 3

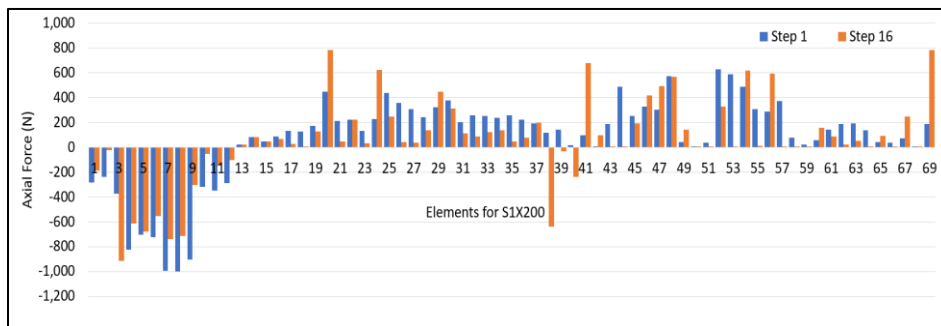
Figure 4 shows the NOF is gradually decreasing and, at the final step, achieving zero. The computational steps increase when the distance of the targeted coordinates from the original nodal coordinates increases. All the analysis cases show the shape change algorithm is effective for the model to approach the final coordinate at different steps. The program was terminated at criteria (i) at least objective function  $< 0.5$ . A small limit value for force elongation will result in greater iterations for a larger final coordinate displacement. Figure 4 depicts the direct relationship between force elongation and displacement magnitude. The shape change process also reveals the occurrence of axial deformation of cables through force elongation.

### 3.4 Axial Force

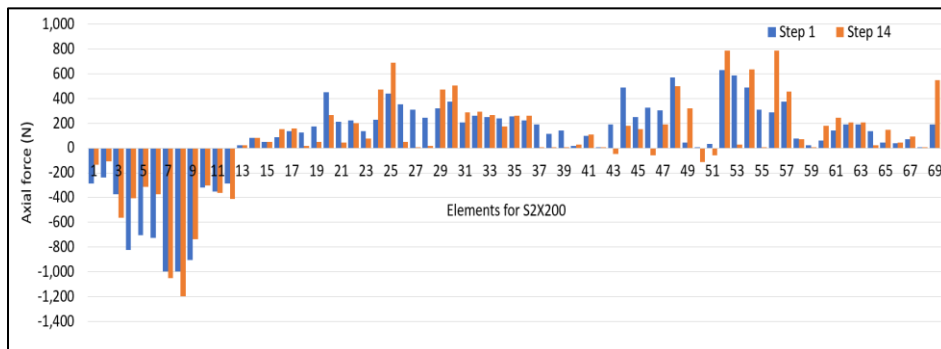
The axial forces of the tensegrity model for cables and struts deal with tensile and compressive forces. Due to their nature of carrying compression forces, the 12 struts (elements 1–12) in this study have a negative axial force. Similarly, the cables experienced positive axial force and were carrying tension throughout the deployment process.

Only the changes in axial force of models with 200 mm increments were outlined in this section. Analysis case S1X200 (Scheme 1) consists of a cluster of undeformed cables from elements 37, 38, 39, 40, 41, and 42. Meanwhile, cables S2X200 (Scheme 2) are made up of a collection of undeformed cables from elements 43, 44, 45, 46, 47, 48, 49, 50, and 51. Finally, the case S3X200 (Scheme 3) consists of undeformed cables from elements 52, 53, 54, 55, 56, 57, 58, 59, and 60.

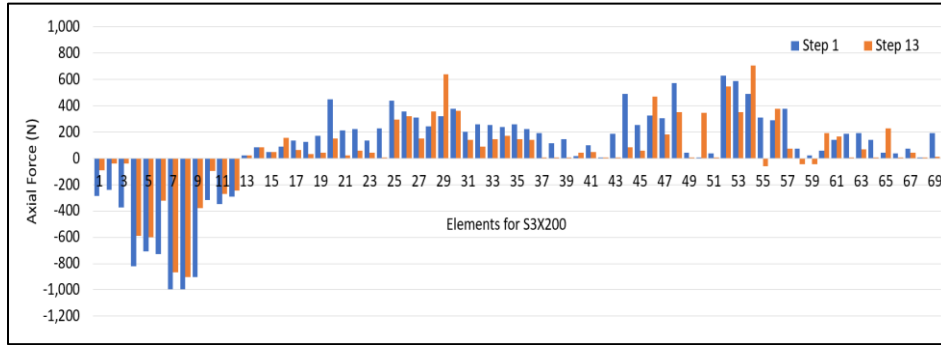
Figure 5 shows the axial forces for all elements at the first and final computational steps. As shown in the bar charts, elements 13, 14 and 15 showed no variations in axial force at the initial and final steps, as they were treated as support at the model’s base. These were stimulated by the horizontal cable’s degree of freedom (DOF) at the base being restrained by the boundary condition of a fixed support in the  $x$ -,  $y$ -, and  $z$ -directions.



(a)



(b)



(c)

**Figure 5.** Axial force at initial and final step of the elements for model  
(a) S1X200, (b) S2X200, (c) S3X200

The axial forces were checked against the yielding of cable elements, and the compressive forces of the strut’s elements were tested against Euler’s buckling load. Axial forces in cables are ensured within the limits in Equation (3).

$$0 \leq n_c \leq \sigma_c A_c \tag{3}$$

And the axial forces in struts are ensured within the limits, as in Equation (4).

$$\max \left\{ -\frac{\pi^2 E_s I_s}{l_s^2}, -\sigma_s A_s \right\} \leq n_s \leq \sigma_s A_s \tag{4}$$

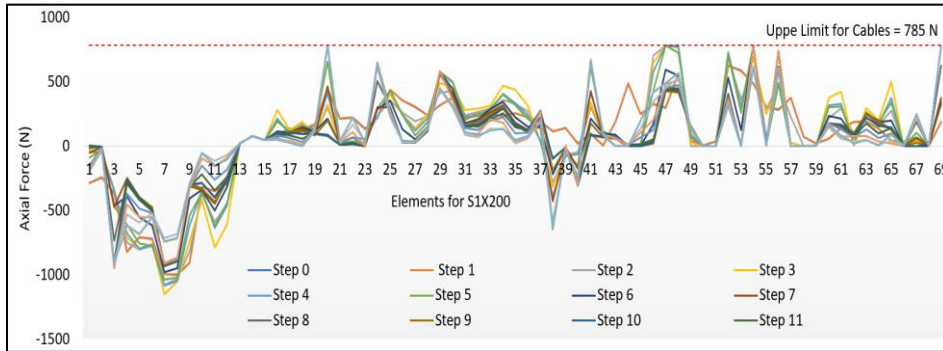
From Equations (3) and (4), the maximum axial force for cable is 785 N, while the maximum value for axial forces for struts is 2525.8 N. The strut’s lower limit of axial force varies for each element depending on its length. Table 5 shows the lower bounds for the axial force limits for each strut’s elements.

**Table 5.** Lower limit for strut axial force using Euler’s Buckling

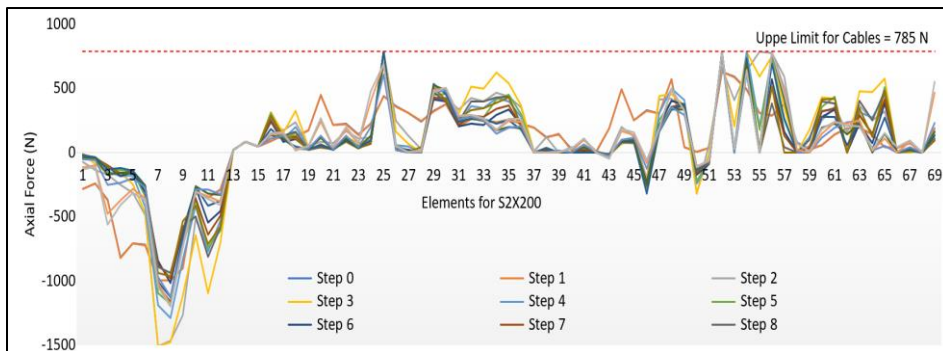
Strut Element Number	Length (mm)	Lower bound axial force limit (N)
1	153.20	- 16,919.76
2	157.80	- 15,929.86
3	147.00	- 18,371.00
4	332.30	- 3,595.18
5	341.10	- 3,412.13
6	306.80	- 4,218.49
7	220.10	- 8,192.96
8	213.60	- 8,698.40
9	198.90	- 10,035.00
10	51.29	- 149,125.63
11	60.18	- 109,613.92
12	56.75	- 123,273.38

Based on Figure 6, all the strut’s elements (Elements 1–12) met the Euler buckling limits because the axial forces applied to the compression element did not exceed the upper and lower bounds. The maximum allowable cable forces are shown in a dashed line. However, some cable elements in each deployment scheme experienced slack behaviour.

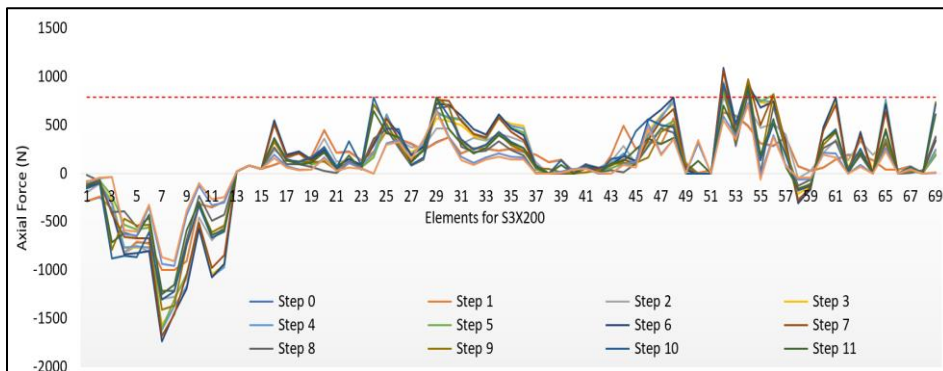
The forces in elements 20, 38, 40, and 69 of Scheme S1 exceeded the force limit and remained as slack cables at the final step. Furthermore, the cables of Scheme S2 whereby Elements 25, 43, 46, 50, 51, 52, 54, 55, and 56 achieved the force limit, but only Elements 54 and 55 can return in tension at the end of the deployment process. For Scheme S3, elements 24, 29, 54, 55, 56, 58, and 59 behaved similarly to slackened cables, but only elements 24 and 46 returned to allowable ranges at the final deployment step.



(a)



(b)



(c)

**Figure 6.** Axial force at incremental steps for  
 (a) S1X200 (b) S2X200 and (c) S3X200

A few cables that fell outside the allowable ranges continued to develop sagging, and the slackened cables that carried negative axial forces could modulate the strut's behaviour.

## 5. Conclusions

Sequential quadratic programming was used as a mathematical method to study how a spine bio-tensegrity model bends and deforms at different deployment schemes. The fundamental algorithm of the computational method is used to perform shape change analysis for the tensegrity model at four different stages.

The computational method iterates to find the optimum solution for the force elongation of the cables of the bio-tensegrity model's during the shape change analysis. The optimisation process for the force elongation ensures the active cables can actuate under prescribed constraints. The study conclusively demonstrates that the algorithm effectively achieves convergence of the solutions, enabling the attainment of the target state across various deployment scenarios.

The numerical application is proven through a total of nine analysis cases at three deployment schemes for a spine bio-tensegrity model to reach the target coordinates in uni-directional modes. The model shows their flexibility trait to exhibit bending deformations at the final state by twisting, bending, rotating, folding and axial deformations throughout the shape change process.

All analysis cases show almost perfect convergence at different computational steps against the normalised objective function (NOF). A direct relationship exists between the computational steps and the target displacement of a tensegrity model. The greater the target displacement, the higher the computational steps. In addition, deployment scheme S3 is the most efficient in achieving the targets observed for all cases that deal with different target displacements.

It has been proven that all strut elements in the bio-tensegrity model carry compression axial force and satisfy the Euler constraints. However, a few cable elements were found to be slackened during the shape change process. Few of the observed cables could return to tensile behaviour before reaching the final coordinate. Further investigation shall be made to ensure the bio-tensegrity model is able to sustain bending deformation without having repeated slack behaviour.

## Acknowledgements

This research was funded by the Ministry of Higher Education Malaysia, FRGS grant (FRGS/1/2021/TK0/UITM/02/11). In addition, the authors would also like to thank the School of Civil Engineering, College of Engineering, Universiti Teknologi MARA, Shah Alam, Selangor.

## Declaration of Conflicting Interests

All authors declare that they have no conflicts of interest.

## References

- H. Chen, F. Zhu, K.I. Jang, X. Feng, J.A. Rogers, Y.H. Zhang. (2018). The equivalent medium of cellular substrate under large stretching, with applications to stretchable electronics, *J. Mech. Phys. Solids* 120, 199–207.
- H. Shang, D. Wei, R. Kang, Y. Chen. (2018). Gait analysis and control of a deployable robot, *Mech. Mach. Theory* 120.
- C. Shi, H.W. Guo, M. Li, R.Q. Liu, Z.Q. Deng. (2018). Conceptual configuration synthesis of line-foldable type quadrangular prismatic deployable unit based on graph theory, *Mech. Mach. Theory* 121, 563–582.
- R. Liu, Y.A. Yao, Y.Z. Li. (2020). Design and analysis of a deployable tetrahedron-based mobile robot constructed by Sarrus linkages, *Mech. Mach. Theory* 152.

- M.C. Phocas, E.G. Christoforou, P. Dimitriou. (2020). Kinematics and control approach for deployable and reconfigurable rigid bar linkage structures, *Eng. Struct.* 208.
- Kan Z, Peng H, Chen B, Zhong W. (2017). Nonlinear dynamic and deployment analysis of clustered tensegrity structures using a positional formulation FEM. *Compos Struct* [Internet]. 2018;187(November 2017):241–58. Available from: <https://doi.org/10.1016/j.compstruct.2017.12.050>
- Oh CL, Choong KK, Low CY. (2012). Biotensegrity inspired robot - Future construction alternative. *Procedia Eng*;41(Iris):1079–84.
- Pellegrino, S., & Calladine, C. R. (1986). Matrix analysis of statically and kinematically indeterminate frameworks. *International Journal of Solids and Structures*, 22(4), 409-428.
- Motro, R. (2011). Structural morphology of tensegrity systems. *Meccanica* 46,27–40.
- Snelson, K. (2012). The art of tensegrity. *Int. J. Space Struct.* 27, 71–80. Al Sabouni-Zawadzka, A.; Gilewski, W. Inherent Properties of Smart Tensegrity Structures. *Appl. Sci.* **2018**, 8, 787.
- Sultan, C., and Skelton, R. (2003). Deployment of tensegrity structures. *Int. J. Solids Struct.* 40, 4637–4657.
- Csölleová, Z. (2012). The analyses of triangular tensegrity prisms' pairs. *Proc. Eng.* 40, 74–78.
- Fest, E., Shea, K., and Smith, I. F. C. (2004). Active tensegrity structure. *J. Struct. Eng.* 130, 1454–1465.
- Motro, R., Maurin, B., and Silvestri, C. (2006). “Tensegrity rings and the hollowrope,” in *IASS Symposium Beijing China* (Beijing), 1–12.
- Skelton, R. E., Adhikari, R., Pinaud, J.-P., and Chan, W. L. (2001). “An introduction to the mechanics of tensegrity structures,” in *Conference on Decision and Control* (Orlando, FL), 4254–4259.
- Schlaich, M. (2003). Der Messeturm in Rostock - ein Tensegrityrekord. *Stahlbau* 72, 697–701.
- Schenk, M., Guest, S., and Herder, J. (2007). Zero stiffness tensegrity structures. *Int. J. Solids Struct.* 44, 6569–6583.
- Averseng, J., and Dubé, J. (2012). Design, analysis and self stress setting of a lightweight deployable tensegrity modular structure. *Proc. Eng.* 40, 14–19.
- Amendola, A., Carpentieri, G., de Oliveira, M., Skelton, R., and Fraternali, F. (2014). Experimental investigation of the softening stiffening response of tensegrity prisms under compressive loading. *Compos. Struct.* 117, 234–243.
- Sultan, C. (2014). Tensegrity deployment using infinitesimal mechanisms. *Int. J. Solids Struct.* 51, 3653–3668.
- Nadia Farhana AH, Oh CL, Yee MH, Anizahyati A. (2018). Overview on the Form-Finding of Tensegrity Structure. *Int J Eng Technol.* 2018;7(3.36):52.
- Oh CL, Choong KK, Nishimura T, Kim JY, Hassanshahi O. (2019). Shape change analysis of tensegrity models. *Lat Am J Solids Struct.* 2019;16(7):1–19.
- Jung E, Ly V, Cessna N, Ngo ML, Castro D, Sunspiral V, et al. Bio-inspired tensegrity flexural joints. *Proc - IEEE Int Conf Robot Autom.* 2018;2(c):5561–6.
- Oh CL, Choong KK, Nishimura T, Kim JY. (2020). Form-finding of spine inspired biotensegrity model. *Appl Sci.* 2020;10(18):1–20.
- Swanson, R.L. (2013). Bio tensegrity: A unifying theory of biological architecture with applications to osteopathic practice, education, and research-a review and analysis. *J. Am. Osteopath. Assoc.* 2013; 113,34–52.
- Veuve N, Sychterz AC, Smith IFC. Adaptive control of a deployable tensegrity structure. *Eng Struct* [Internet]. 2017;152:14–23.